Exact BER Performance for Symbol-Asynchronous Two-User Non-Orthogonal Multiple Access

Chang Liu, *Graduate Student Member, IEEE*, and Norman C. Beaulieu, *Life Fellow, IEEE*

***Abstract*— Two-user non-orthogonal multiple access systems with quadrature phase-shift keying modulation are studied. A time asynchronous scheme for successive interference cancellation receivers that maximally suppresses the inter-user interference compared to any other time asynchronous schemes is proposed. Exact bit error rate (BER) solutions for the two users operating in the additive white Gaussian noise channel using the proposed scheme are derived. A simpler closed-form BER approximation for the weaker user is also presented. Compared to the symbol-synchronous scheme, numerical results show the proposed asynchronous scheme reduces the BER for the stronger signal by a factor of one-half.**

***Index Terms*— Asynchronous transmission, non-orthogonal multiple access (NOMA), successive interference cancellation (SIC), bit error rate (BER).**

I. Introduction

IN PURSUIT of the high data rates demanded in the fifth-generation (5G) networks, non-orthogonal multiple access (NOMA), is regarded as a promising technology to effectively improve the user capacity [1]. Since multiple users share the same time and frequency resources in NOMA, the development of multiuser detection theory is essential to evaluate the system performance. The successive interference cancellation (SIC) receiver is most frequently employed for its advantage of low processing complexity, and a considerable amount of works can be found on evaluating the error rate performance of SIC receivers in power-domain NOMA. Particularly, with quadrature phase-shift keying (QPSK) modulation, the bit error rate (BER) performance for two uplink users with constant channel gains are derived in [2], the BER performance for two or three downlink users in Nakagami-m fading channels is analyzed in [3], and a generalized work on the average BER analysis for any number of downlink users with binary phase-shift keying modulation in Rayleigh fading channels is reported in [4]. In addition, symbol error rate (SER) performance for two downlink quadrature amplitude modulation (QAM) receivers in Rayleigh fading channels is presented in [5] with power allocation constraints, and also the case with pulse amplitude modulation is considered in [6].

Manuscript received October 20, 2020; revised November 14, 2020; accepted November 15, 2020. Date of publication November 18, 2020; date of current version March 10, 2021. The associate editor coordinating the review of this letter and approving it for publication was J. Seo. *(Corresponding author: Chang Liu.)*

The authors are with the Beijing Key Laboratory of Network System Architecture and Convergence, Beijing University of Posts and Telecommunications, Beijing 100876, China, and also with the School of Information and Communication Engineering, Beijing University of Posts and Telecommunications, Beijing 100876, China (e-mail: charinneliu@bupt.edu.cn; nborm@bupt.edu.cn).

Digital Object Identifier 10.1109/LCOMM.2020.3038951

In the aforementioned works, the assumption of perfect synchronization of the user symbols is made in common. However, symbol-synchronous NOMA is not the best strategy. The schemes for asynchronous NOMA proposed in [7]–[10] show that the inter-user interference is significantly suppressed by adding intentional time delays between the user signals, and higher user sum rates are thus attained than those obtained by symbol-synchronous NOMA. The authors in [11] proposed a novel "Triangular" SIC (T-SIC) pattern for uplink asynchronous signal detection, and the BER and capacity performances are analyzed. However, the BER analysis in [11] for symbol-asynchronous NOMA is only asymptotically precise, because 1) the (residual) interference from other users is approximately modeled by a Gaussian distribution, and 2) the correlation between the noise samples that corrupt the overlapped user symbols has been ignored.

To fill this gap, we propose the optimal time-offset to maximally suppress the inter-user interference for two-user asynchronous NOMA with QPSK T-SIC receiver. Analytical BER formulas for both users are derived considering the interference cancellation errors of the stronger user, which means the BER for the weaker user is calculated taking into account all the outcomes of the detection states of the stronger user signal, i.e., the cases of both the correct and the erroneous detection of the stronger signal. Simulation validates the obtained BER formulas.

II. System Model and Detection Criterion

A. Symbol-Asynchronous NOMA

Consider an asynchronous uplink NOMA system with user 1 and user 2 transmitting Gray code QPSK signals to the base station (BS). We assume the multiplicative gains h_1 and h_2 for the channels respectively between user 1, user 2 and the BS are constant scalars, which means no relative phase rotation exists between the two user signals. In this sense, the receiver operates the detection of the in-phase (I) and quadrature (Q) bit streams independently for the received signal. The signal from user 2 is always delayed by $\tau = \eta T$, where T is the symbol duration and $\eta \in [0, 1)$ is the percentage of the symbol time that the symbol streams of user 2 are delayed.[1] Focusing on the I-branch, the received signal envelope is given by

$$y(t) = h_1 d(t) + h_2 s(t - \tau) + n(t) \tag{1}$$

[1]In order to make a theoretical analysis tractable, it is assumed here that the timing difference between two multiuser signals can be adjusted within one symbol duration. A reviewer has pointed out that this is an ideal condition that cannot be implemented in current practical systems [12]. However, current theory in the literature makes this assumption for analytical tractability [7], [10], establishing theoretical benchmarks. In addition, the proposed scheme is achievable in practical downlink implementations as done in [8], [9], [13].

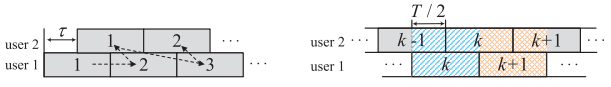

(a) Detection order of the misaligned symbols.

(b) The overlapped parts of s_{k-1}, s_k, s_{k+1} with d_k, d_{k+1}.

Fig. 1. Illustrations of the received symbol sequences.

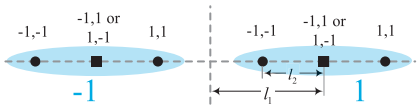

Fig. 2. The joint constellation diagram for the I-branch signal in (3). The two ellipses respectively enclose the signal points that map to $d_k = -1$ and 1. The values of $\{s_{k-1}, s_k\}$ are marked above each signal point.

where $d(t) = \sum_{i=-\infty}^{+\infty} \sqrt{P_1/2}\, d_i r(t - iT)$ and $s(t) = \sum_{i=-\infty}^{+\infty} \sqrt{P_2/2}\, s_i r(t - iT)$ are, respectively, the baseband signals of user 1 and user 2, $\sqrt{P_j}$ is the transmitter power of user j ($j = 1, 2$), $r(t)$ is the power-normalized rectangular pulse[2] with amplitude $1/\sqrt{T}$, d_i and $s_i \in \{1, -1\}$ are respectively the ith I-branch symbols of user 1 and user 2, which map to bits $\{0, 1\}$, and $n(t)$ is an addtive white Gaussian noise (AWGN) process with two-sided spectrum density $N_0/2$. We assume the parameters h_1 and h_2 can be perfectly recovered at the receiver.

To detect the asynchronous user symbols, the receiver utilizes the T-SIC algorithm given in [11]. The detailed process is depicted as follows. Suppose user 1 has larger received power, i.e., $P_1 |h_1|^2 > P_2 |h_2|^2$. The process starts by detecting the first two symbols in the sequence of user 1 signal in succession. Then the first symbol of user 2 is detected after subtracting the remodulated signals of the two detected symbols of user 1 from the received signal, followed by detecting the third symbol in the sequence of user 1, and then the second symbol of user 2 after subtracting the remodulated signal of the third symbol of user 1 from the received signal, etc. The detection order is illustrated in Fig. 1(a).

B. The Optimal Time-Offset and Signal Detection for User 1

Let $l_1 = |h_1| \sqrt{P_1/2}$, $l_2 = |h_2| \sqrt{P_2/2}$ respectively be halves of the minimum distances between the signal points of user 1 and user 2. The kth sample of the output of the I-branch receiver matched filter is given by

$$\begin{aligned} y_k &= \int_{kT}^{(k+1)T} r(t - kT) \{ l_1 d_k r(t - kT) + l_2 [s_{k-1} \\ &\quad \times r(t - \tau - kT + T) + s_k r(t - \tau - kT)] + n(t) \} dt \\ &= l_1 d_k + l_2 [\eta s_{k-1} + (1 - \eta) s_k] + n_k \end{aligned} \tag{2}$$

where $n_k \sim \mathcal{N}(0, N_0/2)$ is the noise sample that appears in the detection of d_k. When $s_{k-1} = s_k$, the interference component $l_2 [\eta s_{k-1} + (1 - \eta) s_k]$ equals $l_2 s_k$ in (2), which is identical to the case of the symbol-synchronous case. However, when $s_{k-1} = -s_k$, the power of the interference component $l_2 [\eta s_{k-1} + (1 - \eta) s_k]$ reduces, and it is clear that $l_2 [\eta s_{k-1} + (1 - \eta) s_k] = 0$ for $\eta = 0.5$. Under this condition, the interference is totally eliminated, and thus the error probability of user 1 equals that of the single user case in the AWGN channel. Observe that this condition occurs for one-half of the signal detection cases since $s_{k-1} = -s_k$ occurs with probability $\frac{1}{2}$. Any other values of η cannot cancel the interference from user 2 completely for $s_{k-1} = -s_k$. Therefore, $0.5T$ is the optimal time-offset in the considered scenario. By applying $\tau = 0.5T$, (2) can be rewritten as

$$y_k = l_1 d_k + 0.5 l_2 (s_{k-1} + s_k) + n_k. \tag{3}$$

Fig. 2 illustrates the joint signal constellation of the noiseless y_k with $\tau = 0.5T$, where each round signal point appears with probability $\frac{1}{8}$, and each square signal point appears with probability $\frac{1}{4}$. Comparing to the constellation diagram of the symbol-synchronous case, the square constellation points newly emerge. The kth estimate of user 1 is obtained by hard-decision $\hat{d}_k = \text{sgn}\{y_k\}$, where $\text{sgn}\{\cdot\}$ is the signum function.

C. Signal Detection for User 2

In the detection of s_k, the receiver needs to remove the interference from d_k and d_{k+1} of user 1 which overlaps s_k as shown in Fig. 1(b), using the detected symbol estimates $\hat{d}_k$ and $\hat{d}_{k+1}$. To sample at the correct time, the detector then delays the sampling time by $\tau = 0.5T$, namely, $t' = t - 0.5T$ is applied. Let $e_i = d_i - \hat{d}_i$ denote the error of interference cancellation for d_i ($i = k, k+1$), the output of the matched filter sampled at $t' = (k+1)T$ is given by

$$\begin{aligned} y'_k &= \int_{kT}^{(k+1)T} r(t' - kT) \{ l_1 [e_k r(t' + 0.5T - kT) + e_{k+1} \\ &\quad \times r(t' - 0.5T - kT)] + l_2 s_k r(t' - kT) + n(t' + 0.5T) \} \\ &\quad \times dt' \\ &= 0.5 l_1 (e_k + e_{k+1}) + l_2 s_k + w_k \end{aligned} \tag{4}$$

where $w_k \sim \mathcal{N}(0, N_0/2)$ is the noise random variable that appears in the detection of s_k. Consequently, the kth estimate of user 2 is obtained by hard-decision $\hat{s}_k = \text{sgn}\{y'_k\}$.

Notably, the noise samples w_k, n_k and n_{k+1} obtained respectively in the detection of s_k, d_k and d_{k+1} are dependent for the following reason. From (4), it is clear that

$$\begin{aligned} w_k &= \int_{kT}^{(k+1)T} n(t' + 0.5T) r(t' - kT) dt' \\ &= \int_{(k+0.5)T}^{(k+1.5)T} n(t) r(t - kT - 0.5T) dt \\ &= \int_{(k+0.5)T}^{(k+1)T} 1/\sqrt{T}\, n(t) dt + \int_{(k+1)T}^{(k+1.5)T} 1/\sqrt{T}\, n(t) dt. \end{aligned} \tag{5}$$

The first and second items of (5) are two independent identically distributed (i.i.d.) Gaussian random variables (RVs) with mean 0 and variance $N_0/4$. They respectively correspond to the I-branch noise components which appear in the blue striated and orange checkered domains of s_k in Fig. 1(b) along the basis $r(t' - kT)$, which are also clearly the constituents of n_k

[2]Many current theoretical studies of multiuser NOMA systems [7]–[11], [13], make the simplifying assumption that the received signals are rectangular. A reviewer has pointed out that practical wireless systems cannot use rectangular pulse shapes, so the theoretical results for tractable analyses are approximations that contribute some insights based on ideal conditions. Future studies may aim at overcoming this assumption.

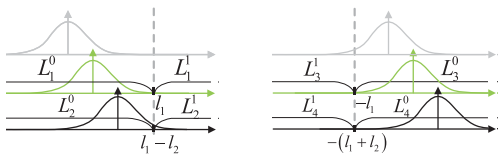

(a) d_k or d_{k+1} is -1. (b) d_k or d_{k+1} is 1.

Fig. 3. The ranges of L_α^m and L_β^q for $\alpha, \beta \in \{1, 2, 3, 4\}$, $m, q \in \{0, 1\}$ with $s_k = 1$. The vertical dashed line represents the decision boundary.

and n_{k+1}, respectively. Now let $n_i^{(1)} = \int_{iT}^{(i+0.5)T} n(t)/\sqrt{T}dt$ and $n_i^{(2)} = \int_{(i+0.5)T}^{(i+1)T} n(t)/\sqrt{T}dt$ be two i.i.d. Gaussian RVs with mean 0 and variance $N_0/4$, then we have $n_k = n_k^{(1)} + n_k^{(2)}$, $n_{k+1} = n_{k+1}^{(1)} + n_{k+1}^{(2)}$ and $w_k = n_k^{(2)} + n_{k+1}^{(1)}$. Consequently, RVs w_k, n_k, n_{k+1} are jointly three-dimensional (3-D) multivariate Gaussian distributed [16, Theorem 5.11.1].

We remark that although the interference can be mitigated with probability 1/2 in the two-user case, this cannot be achieved when more NOMA users access the common channel. Therefore, various, diverse and flexible time-offset schemes may be proposed for the cases with more users.[3]

III. BER Analysis

A. BER of d_k

Without loss of generality, we assume $d_k = 1$ is sent. Thus, the possible joint signal points are those enclosed in the blue ellipse on the right side in Fig. 2. Denote the received signal-to-noise ratios (SNRs) of user 1 and user 2 respectively by $\gamma_1 = \frac{2l_1^2}{N_0} = \frac{|h_1|^2 P_1}{N_0}$ and $\gamma_2 = \frac{2l_2^2}{N_0} = \frac{|h_2|^2 P_2}{N_0}$. Since $\Pr\{s_{k-1} = s_k = 1\} = \Pr\{s_{k-1} = s_k = -1\} = \frac{1}{4}$, and $\Pr\{s_{k-1} = -s_k\} = \frac{1}{2}$, the BER of d_k can be calculated as

$$\begin{aligned} P_d &= \frac{1}{4}\Pr\{n_k < -l_1 + l_2\} + \frac{1}{4}\Pr\{n_k < -l_1 - l_2\} \\ &\quad + \frac{1}{2}\Pr\{n_k < -l_1\} \\ &= \frac{1}{4}\left[Q\left(\sqrt{\gamma_1} - \sqrt{\gamma_2}\right) + Q\left(\sqrt{\gamma_1} + \sqrt{\gamma_2}\right)\right] + \frac{1}{2}Q\left(\sqrt{\gamma_1}\right) \end{aligned} \tag{6}$$

where $Q(x)$ is the Gaussian Q-function [14]. Note the item $Q\left(\sqrt{\gamma_1}\right)$ is the BER of the single user in the AWGN channel. Comparing to the BER of the symbol-synchronous case

$$P_d^0 = \frac{1}{2}\left[Q\left(\sqrt{\gamma_1} - \sqrt{\gamma_2}\right) + Q\left(\sqrt{\gamma_1} + \sqrt{\gamma_2}\right)\right] \tag{7}$$

given by [2, eq. (3)], we have $P_d - P_d^0 = \frac{1}{2}Q\left(\sqrt{\gamma_1}\right) - \frac{1}{4}\left[Q\left(\sqrt{\gamma_1} - \sqrt{\gamma_2}\right) + Q\left(\sqrt{\gamma_1} + \sqrt{\gamma_2}\right)\right] \leq 0$ by using Jensen's inequality [15], where the convexity of $Q(x)$ conditioned on $x > 0$ applies. Thus, it is clearly shown that lower BER of user 1 can be achieved by using the proposed scheme.

[3]For example, one scheme is using a half-symbol duration offset in every other user ranked by their powers to maximally reduce interference from the strongest interferer. A second scheme is using different time offsets weighted on the user powers to reduce as much of the general interference as possible; etc. More insights on downlink multiuser symbol-asynchronous schemes can be found in [13].

TABLE I
Values of the Ranges of L_α^m and L_β^q

$L_1^0 = (b_1^0, u_1^0)$	$L_2^0 = (b_2^0, u_2^0)$	$L_3^0 = (b_3^0, u_3^0)$	$L_4^0 = (b_4^0, u_4^0)$
$(-\infty, l_1)$	$(-\infty, l_1 - l_2)$	$(-l_1, +\infty)$	$(-l_1 - l_2, +\infty)$
$L_1^1 = (b_1^1, u_1^1)$	$L_2^1 = (b_2^1, u_2^1)$	$L_3^1 = (b_3^1, u_3^1)$	$L_4^1 = (b_4^1, u_4^1)$
$(l_1, +\infty)$	$(l_1 - l_2, +\infty)$	$(-\infty, -l_1)$	$(-\infty, -l_1 - l_2)$

B. BER of s_k

From (4), the estimate $\hat{s}_k$ is affected by the noise level w_k and the error introduced by e_k and e_{k+1}. Thus, the BER of s_k can be written as

$$P_s = \Pr\{w_k < -l_2 s_k - 0.5 l_1 (e_k + e_{k+1})\} \tag{8}$$

where e_k and e_{k+1} are respectively determined by d_k, $\hat{d}_k$ and d_{k+1}, $\hat{d}_{k+1}$. Furthermore, $\hat{d}_k$ and $\hat{d}_{k+1}$ are derived from the noise observations of n_k and n_{k+1} given the reference information d_k and d_{k+1}. Therefore, the BER of s_k can be evaluated via summing up the probabilities of the intersections of w_k, n_k and n_{k+1}, where the ranges of n_k and n_{k+1} give different values of e_k and e_{k+1}. Without loss of generality, we assume $s_k = 1$, and $d_k, d_{k+1}, s_{k-1}, s_{k+1} \in \{-1, 1\}$ in the following analysis.

Let $m, q \in \{0, 1\}$ respectively mark the detection status of $\hat{d}_k$ and $\hat{d}_{k+1}$, where number 0 indicates correct detections and number 1 indicates errors. Now denote the range of n_k that leads to detection status m by $L_\alpha^m = (b_\alpha^m, u_\alpha^m)$, and denote the range of n_{k+1} that leads to detection status q by $L_\beta^q = (b_\beta^q, u_\beta^q)$ where b_α^m, b_β^q and u_α^m, u_β^q are respectively the left and right limits of intervals L_α^m and L_β^q, and indices $\alpha = d_k + \frac{5 + s_{k-1}}{2}$, $\beta = d_{k+1} + \frac{s_{k+1} + 5}{2}$ assume values in $\{1, 2, 3, 4\}$ for $d_k, d_{k+1}, s_{k-1}, s_{k+1} \in \{-1, 1\}$. Since $s_k = 1$, the noiseless y_k and y_{k+1} can only be the square signal points and their corresponding right-hand side round signal points in Fig. 2 for d_k and d_{k+1} equal -1 or 1 interchangeably. Thereby, the possible intervals L_α^m, L_β^q for $\alpha, \beta \in \{1, 2, 3, 4\}$ and $m, q \in \{0, 1\}$ are depicted in Fig. 3, and the values of which are listed in Table I. Meanwhile, these noise ranges also correspond to the outcomes of the residual interference components. Let $\mathcal{E}_{\alpha,\beta}^{m,q}$ denote the outcome of the residual interfering symbol $\frac{e_k + e_{k+1}}{2}$ with the value found by

$$\mathcal{E}_{\alpha,\beta}^{m,q} = m\left(2\left\lceil\frac{\alpha}{2}\right\rceil - 3\right) + q\left(2\left\lceil\frac{\beta}{2}\right\rceil - 3\right) \tag{9}$$

where $\lceil\cdot\rceil$ is the round up operator, and $\mathcal{E}_{\alpha,\beta}^{m,q} \in \{-2, -1, 0, 1, 2\}$ for $\alpha, \beta \in \{1, 2, 3, 4\}$ and $m, q \in \{0, 1\}$. The error probability of $\hat{s}_k$ in (8) can be rewritten as

$$\begin{aligned} P_s &= \sum_{m,q \in \varphi} \sum_{d_k, d_{k+1}, s_{k-1}, s_{k+1} \in \chi} \Pr\Big\{w_k < -l_2 s_k - l_1 \mathcal{E}_{\alpha,\beta}^{m,q}, \\ &\qquad n_k \in L_\alpha^m, n_{k+1} \in L_\beta^q \big| d_k, d_{k+1}, s_{k-1}, s_{k+1}, s_k = 1\Big\} \cdot \frac{1}{16} \\ &= \sum_{m=0}^{1}\sum_{q=0}^{1}\sum_{\alpha=1}^{4}\sum_{\beta=1}^{4}\frac{1}{16} \\ &\qquad \times \Pr\left\{w_k < -l_2 - l_1 \mathcal{E}_{\alpha,\beta}^{m,q},\ n_k \in L_\alpha^m, n_{k+1} \in L_\beta^q\right\} \end{aligned} \tag{10}$$

where $\varphi = \{0, 1\}$, $\chi = \{-1, 1\}$. The probability in (10) can be obtained as (11) shown at the bottom of the page, where the dummy variables $g_1 = \frac{z_2+z_3}{\sqrt{2}}$, $g_2 = \frac{z_3-z_2}{\sqrt{2}}$, and the integration region $\mathcal{S} = \left\{ (g_1, g_2) \, | b_\alpha^m + b_\beta^q - g_1 \le g_2 \le g_1 - b_\alpha^m + b_\beta^q \right\}$ for $|u_\alpha^m|, \left|u_\beta^q\right| \to \infty$; $\mathcal{S} = \left\{ (g_1, g_2) \, | g_2 + b_\alpha^m - u_\beta^q \le g_1 \le b_\alpha^m + u_\beta^q - g_2 \right\}$ for $|u_\alpha^m|, \left|b_\beta^q\right| \to \infty$; $\mathcal{S} = \left\{ (g_1, g_2) \, | u_\alpha^m + b_\beta^q - g_2 \le g_1 \le u_\alpha^m - b_\beta^q + g_2 \right\}$ for $|b_\alpha^m|, \left|u_\beta^q\right| \to \infty$; $\mathcal{S} = \left\{ (g_1, g_2) \, | g_1 - u_\alpha^m + u_\beta^q \le g_2 \le u_\alpha^m + u_\beta^q - g_1 \right\}$ for $|b_\alpha^m|$, $\left|b_\beta^q\right| \to \infty$. By integrating g_2 over the corresponding ranges with the transformed bounds and simplifying, (11) results in eq. (12) shown at the bottom of the page. The BER of s_k can be achieved by substituting (12) into (10) with the interval bounds listed in Table I.

Note that the correlation coefficients between w_k and n_k, and w_k and n_{k+1} are both 0.5. By ignoring this weak correlation in (10) and assuming independence instead, a BER approximation for s_k can be derived in closed-form as

$$\begin{aligned} P_s &\approx \sum_{m=0}^{1}\sum_{q=0}^{1}\sum_{\alpha=1}^{4}\sum_{\beta=1}^{4}\frac{1}{16}\Pr\left\{w_k < -l_2 - l_1\mathcal{E}_{\alpha,\beta}^{m,q}\right\} \\ &\quad \times \Pr\left\{n_k \in L_\alpha^m\right\}\Pr\left\{n_{k+1} \in L_\beta^q\right\} \\ &= \sum_{m=0}^{1}\sum_{q=0}^{1}\sum_{\alpha=1}^{4}\sum_{\beta=1}^{4}\frac{1}{16}Q\left(\sqrt{\gamma_2} + \sqrt{\gamma_1}\mathcal{E}_{\alpha,\beta}^{m,q}\right) \\ &\quad \times \left[Q\left(\sqrt{2/N_0}b_\alpha^m\right) - Q\left(\sqrt{2/N_0}u_\alpha^m\right)\right] \\ &\quad \times \left[Q\left(\sqrt{2/N_0}b_\beta^q\right) - Q\left(\sqrt{2/N_0}u_\beta^q\right)\right] \end{aligned} \tag{13}$$

where the values of b_α^m, u_α^m, b_β^q and u_β^q are given in Table I. The approximation in (13) shows intuitively the BER of user 2 is constrained by the residual interference $\mathcal{E}_{\alpha,\beta}^{m,q}$, and is asymptotically linear with the probabilities of the detection status m and q of $\hat{d}_k$ and $\hat{d}_{k+1}$, respectively.

IV. Numerical and Simulation Results

The BER performance for the two users using the proposed symbol-asynchronous NOMA scheme is presented. For comparisons, the BER performance of the symbol-synchronous case obtained in [2] is also presented. Simulation results are given to verify the analytical results, where Gray code QPSK is employed. The noise samples that corrupt the overlapped symbols of user 1 and user 2 are constructed by following the same method of constructing n_k, n_{k+1} and w_k as previously described in Sec. II. All the simulations were carried out in Matlab. The size of each symbol stream of a user sampled at the receiver matched filter is assumed to be 10^6 symbols.

Fig. 4 plots the BERs of user 1 and user 2 versus γ_2 using the proposed scheme and the symbol-synchronous scheme with $\gamma_1 = 10$ dB. It is clear that by using the time-offset scheme, the BER of user 1 is reduced by a factor of one-half comparing to that of the symbol-synchronous case. The reason is the term $\frac{1}{2}Q\left(\sqrt{\gamma_1}\right) = 3.91 \times 10^{-4}$ in (6), is negligible to the value of the sum of the first two items in (6) for -2 dB $\le \gamma_2 \le 10$ dB. By revisiting the derivations in Sec. III-A, we have $P_d \approx \frac{1}{2}P_d^0$. Now focus on the BER performance of user 2. It is seen that the two schemes achieve very close BERs when $\gamma_2 < 3$ dB. This is because the error propagation is relatively insignificant with the noise dominating the BER performance at poor γ_2. However, as γ_2 grows beyond 3 dB, the mutual interference heightens, and the BER performance of user 2 using the proposed scheme deteriorates at a much

$$\begin{aligned} &\Pr\left\{w_k < -l_2 - l_1\mathcal{E}_{\alpha,\beta}^{m,q}, n_k \in L_\alpha^m, n_{k+1} \in L_\beta^q\right\} \\ &= \int_{L_\beta^q}\int_{L_\alpha^m}\int_{-\infty}^{-l_2-l_1\mathcal{E}_{\alpha,\beta}^{m,q}} \frac{1}{2\sqrt{\pi N_0/2}^3}e^{-2\left(z_1 - \frac{z_2+z_3}{2}\right)^2/N_0}dz_1 e^{-\left(z_2^2+z_3^2\right)/N_0}dz_2dz_3 \\ &= \int_{L_\beta^q}\int_{L_\alpha^m}\frac{1}{\pi N_0}Q\left(\frac{z_2+z_3+2l_2+2l_1\mathcal{E}_{\alpha,\beta}^{m,q}}{\sqrt{N_0}}\right)e^{-\frac{z_2^2+z_3^2}{N_0}}dz_2\, dz_3 = \iint\limits_{g_1,g_2\in\mathcal{S}} Q\left(\frac{\frac{g_1}{\sqrt{2}}+l_2+l_1\mathcal{E}_{\alpha,\beta}^{m,q}}{\sqrt{N_0}/2}\right)\frac{1}{\pi N_0}e^{-\frac{g_1^2+g_2^2}{N_0}}dg_1dg_2 \end{aligned}$$

$$\Pr\left\{w_k \le -l_2 - l_1\mathcal{E}_{\alpha,\beta}^{m,q}, n_k \in L_\alpha^m, n_{k+1} \in L_\beta^q\right\} \tag{11}$$

$$= \begin{cases} \displaystyle\int_{\left(b_\alpha^m+b_\beta^q\right)/\sqrt{N_0}}^{+\infty}\left[Q\left(\frac{2b_\beta^q}{\sqrt{N_0}} - g_1\right) - Q\left(g_1 - \frac{2b_\alpha^m}{\sqrt{N_0}}\right)\right]Q\left(g_1 + \sqrt{2\gamma_2} + \sqrt{2\gamma_1}\mathcal{E}_{\alpha,\beta}^{m,q}\right)\frac{e^{-g_1^2/2}}{\sqrt{2\pi}}dg_1, & |u_\alpha^m|, \left|u_\beta^q\right| \to \infty \\ \displaystyle\int_{-\infty}^{\left(b_\alpha^m+u_\beta^q\right)/\sqrt{N_0}} Q\left(\frac{2b_\alpha^m}{\sqrt{N_0}} - g_1\right)Q\left(g_1 + \sqrt{2\gamma_2} + \sqrt{2\gamma_1}\mathcal{E}_{\alpha,\beta}^{m,q}\right)\frac{e^{-g_1^2/2}}{\sqrt{2\pi}}dg_1 & \\ \quad + \displaystyle\int_{\left(b_\alpha^m+u_\beta^q\right)/\sqrt{N_0}}^{+\infty} Q\left(g_1 - \frac{2u_\beta^q}{\sqrt{N_0}}\right)Q\left(g_1 + \sqrt{2\gamma_2} + \sqrt{2\gamma_1}\mathcal{E}_{\alpha,\beta}^{m,q}\right)\frac{e^{-g_1^2/2}}{\sqrt{2\pi}}dg_1 & |u_\alpha^m|, \left|b_\beta^q\right| \to \infty \\ \displaystyle\int_{-\infty}^{\left(u_\alpha^m+u_\beta^q\right)/\sqrt{N_0}}\left[Q\left(g_1 - \frac{2u_\alpha^m}{\sqrt{N_0}}\right) - Q\left(\frac{2u_\beta^q}{\sqrt{N_0}} - g_1\right)\right]Q\left(g_1 + \sqrt{2\gamma_2} + \sqrt{2\gamma_1}\mathcal{E}_{\alpha,\beta}^{m,q}\right)\frac{e^{-g_1^2/2}}{\sqrt{2\pi}}dg_1, & |b_\alpha^m|, \left|u_\beta^q\right| \to \infty \\ \displaystyle\int_{-\infty}^{\left(u_\alpha^m+b_\beta^q\right)/\sqrt{N_0}} Q\left(\frac{2b_\beta^q}{\sqrt{N_0}} - g_1\right)Q\left(g_1 + \sqrt{2\gamma_2} + \sqrt{2\gamma_1}\mathcal{E}_{\alpha,\beta}^{m,q}\right)\frac{e^{-g_1^2/2}}{\sqrt{2\pi}}dg_1 & \\ \quad + \displaystyle\int_{\left(u_\alpha^m+b_\beta^q\right)/\sqrt{N_0}}^{+\infty} Q\left(g_1 - \frac{2u_\alpha^m}{\sqrt{N_0}}\right)Q\left(g_1 + \sqrt{2\gamma_2} + \sqrt{2\gamma_1}\mathcal{E}_{\alpha,\beta}^{m,q}\right)\frac{e^{-g_1^2/2}}{\sqrt{2\pi}}dg_1 & |b_\alpha^m|, \left|b_\beta^q\right| \to \infty \end{cases} \tag{12}$$

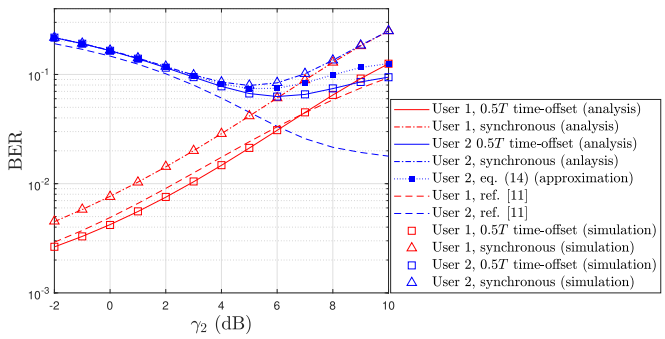

Fig. 4. BER performances of user 1 and user 2 versus γ_2 for $\gamma_1 = 10$ dB.

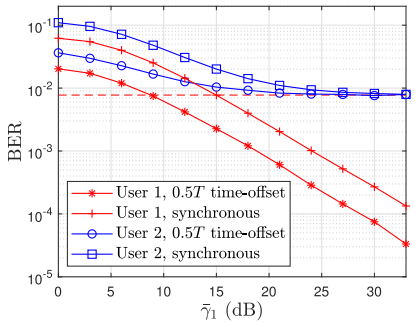

Fig. 5. Average BER performance over flat Rayleigh fading channels versus $\bar{\gamma}_1$ for $\bar{\gamma}_2 = 18$ dB.

slower rate than the one utilizing the symbol-synchronous scheme. Note that in this region, the system becomes sensitive to error propagation. Therefore, it is seen that the symbol-asynchronous scheme suppresses the error propagation effectively. The superiority in BER performance of the proposed scheme is especially obvious when γ_2 approaches γ_1. For example, the BER of user 2 utilizing the proposed scheme is reduced to one third at $\gamma_2 = \gamma_1 = 10$ dB compared to the synchronous case.

Fig. 4 also plots the approximated user BER performance for the proposed asynchronous scheme. It is clear that the solutions given in [11] deviate from the exact BER performances of both users for the reasons specified in Sec. I. In particular, the BER for user 2 given in [11] shows a distant disagreement with the exact BER except for the extreme power-imbalance case, and it can not reveal the asymptotic BER performance for user 2. In sharp contrast, observe that the BER approximation for user 2 proposed in eq. (13) is very tight to the exact BER performance, when the interference is strong. As γ_2 grows larger, the approximation only shows a small deviation from the exact performance. The proposed BER approximation for user 2 is more accurate than the solution given in [11].

Fig. 5 examines the simulated average user BER performance over flat Rayleigh fading channels, versus the average SNR of user 1. The average received SNR, $\bar{\gamma}_j$, for user j equals $\mathbb{E}\{\gamma_j\}$, where $\mathbb{E}\{\cdot\}$ denotes the expected value. The i.i.d. channel gains h_1, $h_2 \sim \mathcal{CN}(0,1)$ are assigned with complex Gaussian random numbers in the simulation. The receiver detects the user with larger instantaneous SNR in priority, i.e., when $\gamma_1 > \gamma_2$, it detects user 1 first, and otherwise, it detects user 2 first. It can be seen from Fig. 5 that utilizing the $0.5T$ time asynchrony, the BER for user 1 has been decreased to roughly 1/3 of the BER for the synchronous case. As to the BER for user 2, still the $0.5T$ time-offset scheme shows a large superiority. With the increase of $\bar{\gamma}_1$, the BER of user 1 keeps decreasing, and the BER of user 2 gradually converges to the BER for the single user case i.e., 7.74×10^{-3} given by [14, eq. (13-3-7)]. In this process, the BER for the $0.5T$ time-offset case converges much faster compared to the average BER for the synchronous case. In general, the proposed asynchronous system needs 6 dB less in $\bar{\gamma}_1$ to achieve the same BER performance for the synchronous case.

V. Conclusion

In this letter, a half-symbol duration time-offset transmission scheme was proposed for two QPSK user signals in NOMA. Exact BER formulas for the two users were derived. Benefitting from the proposed time-offset implementation, the BER for the stronger user is nearly always reduced by a factor of one-half when the interference power is non-negligible. The BER of the weaker user is also reduced. The simulated average BER performance for users over flat Rayleigh channels show the proposed scheme outperforms the synchronous scheme by larger margins than in the AWGN channel case.

References

[1] L. Dai *et al.*, "A survey of non-orthogonal multiple access for 5G," *IEEE Commun. Surveys Tuts.*, vol. 20, no. 3, pp. 2294–2323, 3rd Quart., 2018.
[2] X. Wang *et al.*, "Closed-form BER expressions of QPSK constellation for uplink non-orthogonal multiple access," *IEEE Commun. Lett.*, vol. 21, no. 10, pp. 2242–2245, Oct. 2017.
[3] T. Assaf *et al.*, "Exact BER performance analysis for downlink NOMA systems over Nakagami-m fading channels," *IEEE Access*, vol. 7, pp. 134539–134555, 2019.
[4] M. Aldababsa *et al.*, "Bit error rate for NOMA network," *IEEE Commun. Lett.*, vol. 24, no. 6, pp. 1188–1191, Jun. 2020.
[5] I.-H. Lee and J.-B. Kim, "Average symbol error rate analysis for non-orthogonal multiple access with M -Ary QAM signals in Rayleigh fading channels," *IEEE Commun. Lett.*, vol. 23, no. 8, pp. 1328–1331, Aug. 2019.
[6] Q. He *et al.*, "Closed-form symbol error rate expressions for non-orthogonal multiple access systems," *IEEE Trans. Veh. Technol.*, vol. 68, no. 7, pp. 6775–6789, Jul. 2019.
[7] M. Ganji and H. Jafarkhani, "Interference mitigation using asynchronous transmission and sampling diversity," in *Proc. IEEE Global Commun. Conf. (GLOBECOM)*, Washington, DC, USA, Dec. 2016, pp. 1–6.
[8] J. Cui *et al.*, "Asynchronous NOMA for downlink transmissions," *IEEE Commun. Lett.*, vol. 21, no. 2, pp. 402–405, Feb. 2017.
[9] M. Ganji and H. Jafarkhani, "Time asynchronous NOMA for downlink transmission," in *Proc. IEEE Wireless Commun. Netw. Conf. (WCNC)*, Marrakech, MO, USA, Apr. 2019, pp. 1–6.
[10] X. Zou *et al.*, "An analysis of two-user uplink asynchronous non-orthogonal multiple access systems," *IEEE Trans. Wireless Commun.*, vol. 18, no. 2, pp. 1404–1418, Feb. 2019.
[11] H. Haci *et al.*, "Performance of non-orthogonal multiple access with a novel asynchronous interference cancellation technique," *IEEE Trans. Commun.*, vol. 65, no. 3, pp. 1319–1335, Mar. 2017.
[12] *NR, Phys. Layer Procedures for Control*, document 38.213 v15.5.0, 3GPP, May 2019.
[13] M. Ganji *et al.*, "Exploiting time asynchrony in multi-user transmit beamforming," *IEEE Trans. Wireless Commun.*, vol. 19, no. 5, pp. 3156–3169, May 2020.
[14] J. G. Proakis and M. Salehi, *Digital communications*, vol. 4. New York, NY, USA: McGraw-hill, 2001.
[15] A. N. Shiryayev, *Probability*. New York, NY, USA: Springer-Verlag, 1984.
[16] M. Fisz, *Probability Theory and Mathematical Statistics*, 3rd ed. New York, NY, USA: Wiley, 1967.